Journal of Luminescence 221 (2020) 117032

Contents lists available at ScienceDirect

Journal of Luminescence

journal homepage: http://www.elsevier.com/locate/jlumin

Polarized emission from single perovskite $FAPbBr_3$ nanocrystals

Jinqiu Liu [a], Fengrui Hu [a,**], Yong Zhou [a], Chunfeng Zhang [a], Xiaoyong Wang [a,*], Min Xiao [a,b]

[a] National Laboratory of Solid State Microstructures, Collaborative Innovation Center of Advanced Microstructures, College of Engineering and Applied Sciences, and School of Physics, Nanjing University, Nanjing, 210093, China
[b] Department of Physics, University of Arkansas, Fayetteville, AR, 72701, USA

ARTICLE INFO

Keywords:
Lead-halide perovskite
$FAPbBr_3$
Nanocrystals
Polarized emission

ABSTRACT

Owing to the superior performance of lead-halide perovskites in various optoelectronic devices, their low-dimensional counterparts of quantum-confined nanocrystals (NCs) have started drawing intensive research attention. Here we report a systematic study on the optical properties of single $FAPbBr_3$ NCs, which demonstrate high-purity single-photon emission, large absorption cross-section and narrow photoluminescence linewidth. Interestingly, linearly-polarized emission can be partially observed in single $FAPbBr_3$ NCs at the room temperature, the degree of which is significantly enhanced at the cryogenic temperature. The above polarization phenomenon is attributed to the large energy-level splitting of the bright-exciton states, leading to efficient exciton recombination from the lowest state with a 1D dipole moment. This unique feature of linear polarization in the optical emission of single $FAPbBr_3$ NCs has not only provided a deep understanding of their exciton energy-level structures, but also suggested potential polarization-oriented applications such as in photodetectors, light-emitting diodes and lasers.

1. Introduction

The chemical formula of lead-halide perovskites can be generally described as $APbX_3$, where A is a cation (Cs, methylammonium (MA) or formamidinium (FA)) and X is a halogen (Cl, Br, or I). Inspired by the superior performance of lead-halide perovskites in various optoelectronic devices, their low-dimensional structures have been recently synthesized in the forms of organic-inorganic hybrid [1,2] and all-inorganic [3] nanocrystals (NCs). The exciton energies of lead-halide perovskite NCs are strongly dependent on their sizes, resulting in the tunable optical emission from ~410 to 700 nm across the whole visible spectrum [3–6]. In addition, lead-halide perovskite NCs in the colloidal phase can be easily dissolved in different solvents to enable a flexible tuning of the halide compositions through the anion exchange reaction [7,8]. With the subsequent achievements in realizing precise size control [9] and ion doping [10] in lead-halide perovskite NCs, great research efforts are now being devoted to the investigation of their exciton recombination dynamics by means of transient absorption and time-resolved photoluminescence (PL) measurements at the ensemble level [11,12]. Meanwhile, single-particle spectroscopic technique has also been applied on lead-halide perovskite NCs, revealing novel optical properties such as high-purity single-photon emission, suppressed PL blinking and spectral diffusion, and the energy-level fine structures of band-edge excitons [13–22]. Accompanying the above fundamental studies, low-threshold lasers [23–25] and high-efficiency light-emitting diodes [26,27] have also been fabricated from lead-halide perovskite NCs to advance their potential applications in nano-optoelectronic devices.

In contrast to the well-studied all-inorganic perovskite lead-halide NCs, the organic-inorganic hybrid ones are now subjected to fewer research explorations due to their relatively poor chemical and thermal stabilities. Following the successful synthesis of FA lead-halide perovskite NCs ($FAPbX_3$) with a PL quantum yield as high as 85% [2,4,5,28], a bunch of interesting optical properties have been demonstrated, mainly including single-photon emission [29,30], exciton fine-structure splitting [31,32], room-temperature charged-exciton species [33] and strong exciton-phonon coupling [31,34]. In this work, we report a systematic study on the optical properties of single $FAPbBr_3$ NCs, such as single-photon emission, large absorption cross section, charged-exciton emission and narrow PL linewidth. Interestingly, the degree of linear polarization as large as ~21% can be observed in the optical emission of single $FAPbBr_3$ NCs at the room temperature, which is enhanced to

* Corresponding author.
** Corresponding author.
E-mail addresses: frhu@nju.edu.cn (F. Hu), wxiaoyong@nju.edu.cn (X. Wang).

https://doi.org/10.1016/j.jlumin.2020.117032
Received 4 September 2019; Received in revised form 19 December 2019; Accepted 5 January 2020
Available online 7 January 2020

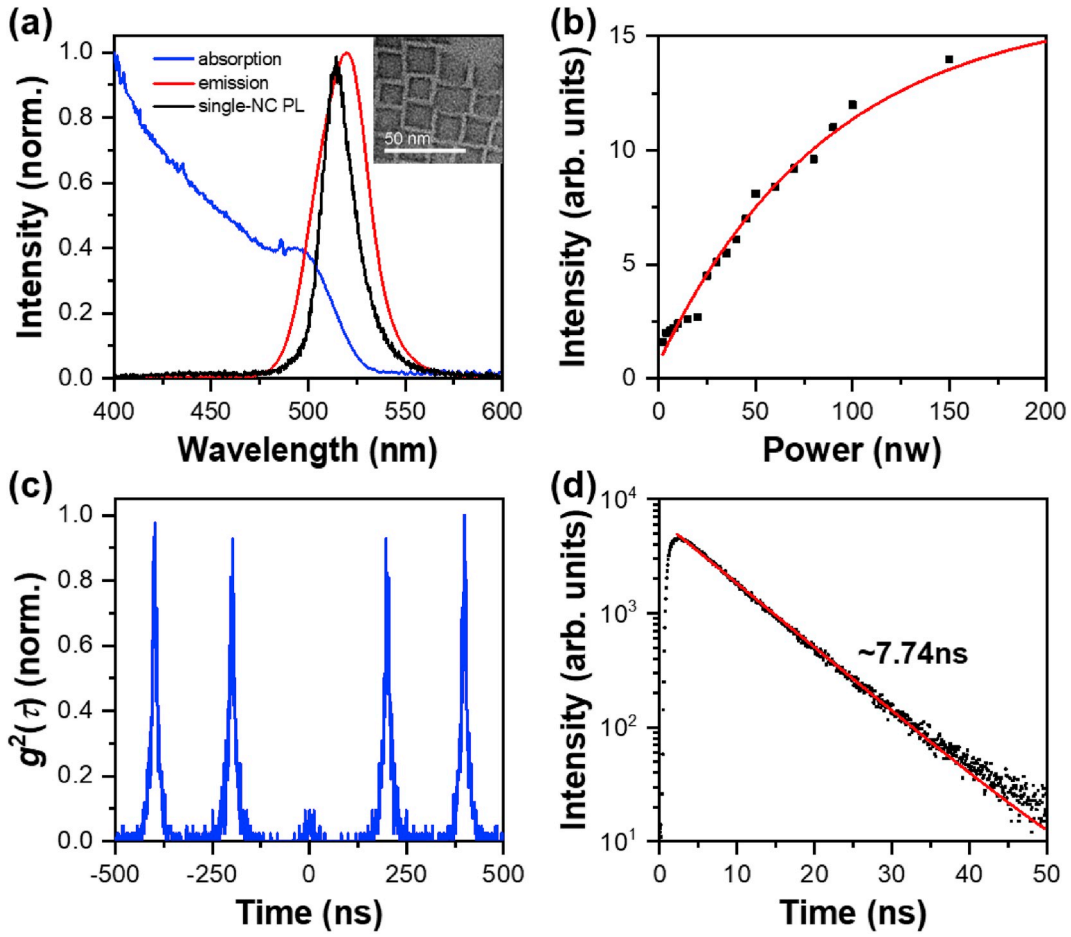

Fig. 1. (a) Solution absorption and emission spectra measured for ensemble $FAPbBr_3$ NCs, together with the PL spectrum measured for a single $FAPbBr_3$ NC. Inset: TEM image of several single $FAPbBr_3$ NCs with an average edge length of ~12 nm. (b) PL intensity of a single $FAPbBr_3$ NC measured as a function of the laser excitation power, and fitted by the solid line with the function form of $I \propto 1 - e^{-<N>} = 1 - e^{-j\sigma}$. (c) Second-order photon correlation function measured for a single $FAPbBr_3$ NC with a $g^2(\tau)$ value of ~0.09 estimated at $\tau = 0$. (d) PL decay curve measured for a single $FAPbBr_3$ NC and fitted by a single-exponential function with an exciton recombination lifetime of ~7.74 ns. All the above measurements were performed at the room temperature.

~92% at the cryogenic temperature of 4 K. This linearly-polarized optical emission observed even at the room temperature is attributed to the large energy-level splitting of the bright-exciton states, leading to efficient exciton recombination from the lowest state carrying a 1D dipole moment in the optical transition.

2. Experiment methods

To prepare the FA-oleate precursor, 0.521 g Formamidinium acetate and 20 mL oleic acid were dried at 120 °C under vacuum inside a 100 mL three-neck flask. After being heated to 130 °C under N_2 until the reaction was completed, the above mixture was then cooled to 50 °C and dried for 30 min under vacuum. For the subsequent synthesis of $FAPbBr_3$ NCs, 5 mL octadecene and 0.069 g $PbBr_2$ were loaded into a 25 mL three-neck flask, and dried for 1 h at 120 °C under vacuum. 0.5 mL oleylamine and 1 mL oleic acid were then added into the flask at 120 °C under N_2 after being dried. As the $PbBr_2$ powder was completely dissolved, the temperature was raised to 160 °C and 2.5 mL FA-oleate precursor prepared above was quickly injected into the flask. After 5 s, the solution was cooled in ice-water bath to stop the reaction. The product was centrifuged for 5 min at 12000 rpm with the added 10 mL toluene and 5 mL acetonitrile. The precipitate was re-dispersed in 5 mL toluene and centrifuged again for 5 min at 4000 rpm, after which the supernatant was collected. The as-synthesized $FAPbBr_3$ NCs have a cubic shape with an average edge length of ~12 nm [35], as can been seen from the TEM image shown in the inset of Fig. 1(a).

For the optical measurements at room temperature, one drop from the diluted toluene solution containing the polymer of poly-DL-lactide and $FAPbBr_3$ NCs was spin-coated onto a fused silica substrate, which was placed in a confocal scanning optical microscope. The output beam from a 405 nm ps pulse laser with a repetition rate of 5 MHz was focused onto the sample surface through an immersion-oil objective with a numerical aperture of 1.4. Optical signal from a single $FAPbBr_3$ NC can be sent either through a spectrometer to the CCD for the PL spectral measurement, or to a pair of avalanche photodiodes (APDs) for the measurement of single-photon emission, PL intensity time trace or PL decay lifetime with a resolution of ~200 ps. For the optical measurements of single $FAPbBr_3$ NCs at the cryogenic temperature of 4 K, quite similar optical setups to the above was employed except that the sample substrate was attached to the cold finger of a helium-free cryostat and the immersion-oil objective was replaced by a dry one with a numerical aperture of 0.95. To characterize the linear polarization of optical emission from a single $FAPbBr_3$ NC, a half-wave plate and a linear polarizer would be inserted into the signal collection path.

3. Results and discussion

We first studied the ensemble and single $FAPbBr_3$ NCs at the room temperature. From the solution measurements, the emission and band-edge absorption peaks of ensemble $FAPbBr_3$ NCs can be estimated from Fig. 1(a) to be located at ~520 nm (~2.38 eV) and ~496 nm (~2.50 eV), respectively. The PL spectrum measured at the room

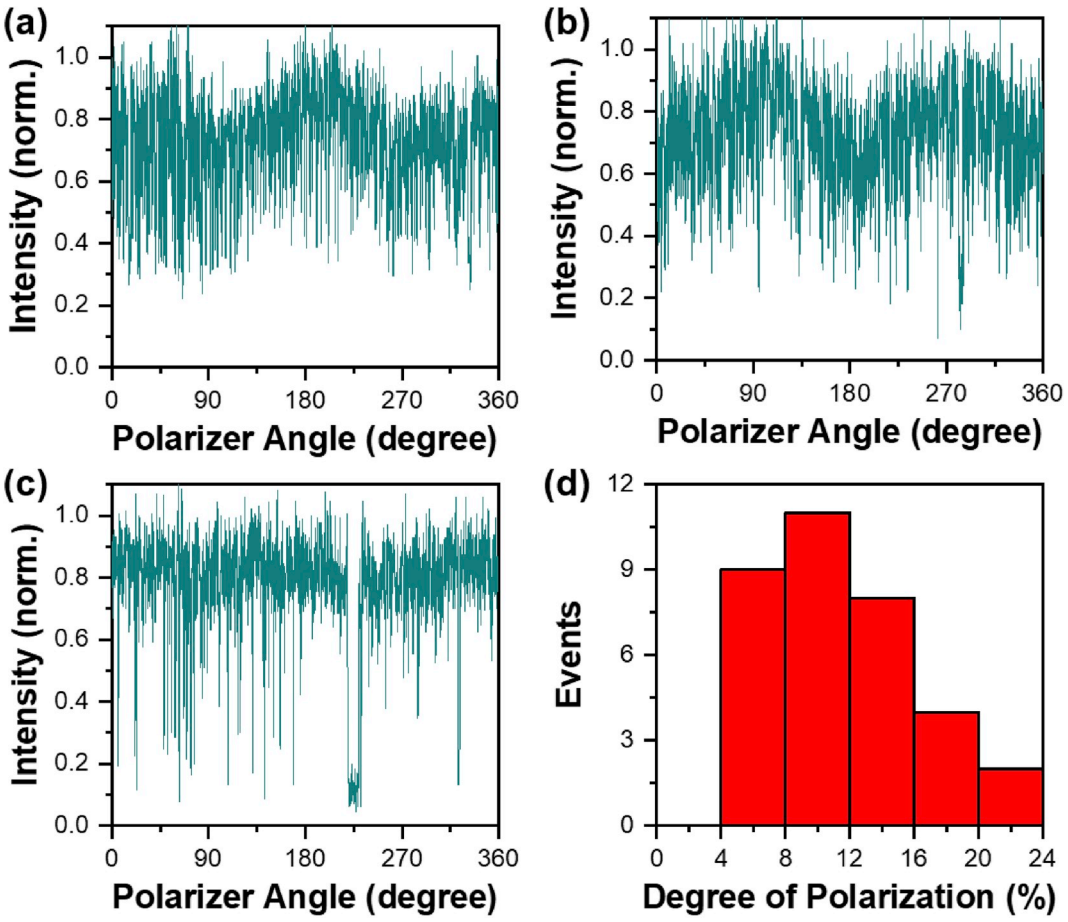

Fig. 2. (a),(b) PL intensities measured for two single $FAPbBr_3$ NCs showing obvious sinusoidal modulations with the changing polarizer angles. (c) PL intensity measured for a single $FAPbBr_3$ NC without being modulated by the changing polarizer angle. (d) Statistical histogram showing the DLP values measured for 34 single $FAPbBr_3$ NCs. Due to random PL intensity fluctuation even in the blinking "on" state, the minimum DLP value that can be resolved for a single $FAPbBr_3$ NC is ~4%. The PL intensity time traces in (a)–(c) were obtained at the room temperature and plotted with a binning time of 100 ms.

temperature for a representative single $FAPbBr_3$ NC is also plotted in Fig. 1(a) with a linewidth of ~18 nm, which is much narrower than that of ~27 nm for the ensemble PL peak. Due to nonradiative Auger recombination of multiple excitons, the PL intensity of a single $FAPbBr_3$ NC would become saturated with the increasing laser excitation power. This PL saturation behavior can be described by the function of $I \propto 1 - e^{-<N>} = 1 - e^{-j\sigma}$, where I is the PL intensity, $<N>$ is the number of exciton created per pulse in a single NC, j is the excitation photon flux and σ is the absorption cross section [16]. Using the above function to fit the PL saturation curve shown in Fig. 1(b) for a single $FAPbBr_3$ NC, we can obtain a value of $\sim 2.19 \times 10^{-13}$ cm^2 for its absorption cross section at 405 nm, which is comparable to that of $\sim 2.23 \times 10^{-13}$ cm^2 estimated previously for single $CsPbBr_3$ NCs [16].

In the following experiments, we always set $<N> = 0.1$ with a low laser power to avoid causing any nonlinear effect due to the generation of multiple excitons and no degradation effect was observed in the single $FAPbBr_3$ NCs during the optical measurement lasting for as long as 30 min. In Fig. 1(c), we plot the second-order photon correlation function measured for a single $FAPbBr_3$ NC, where the $g^2(\tau)$ value of ~0.09 estimated at $\tau = 0$ unambiguously confirms the single-photon emission feature. Being able to emit such high-purity single photons, the single $FAPbBr_3$ NCs studied here, among other types of single perovskite NCs [14–16], can be firmly pushed to the quantum-information-processing regime [36,37] beyond their traditional applications in optoelectronic devices [23–27]. The PL decay curve measured for a single $FAPbBr_3$ NC is plotted in Fig. 1(d), from which an exciton recombination lifetime of ~7.74 ns can be extracted with the single-exponential fitting function. By performing similar PL decay measurements for tens of single $FAPbBr_3$ NCs, an average lifetime value of ~8.4 ns could be obtained.

In Fig. 2(a) and (b), we plot the PL intensities measured for two single $FAPbBr_3$ NCs as a function of the linear polarizer angle tuned slowly with time from 0 to 360°. Attached to a mild fluorescence blinking time trace, a sinusoidal modulation of the PL intensity with the polarizer angle can be clearly observed for each single $FAPbBr_3$ NC. It should be noted that the PL intensity variations of the two $FAPbBr_3$ NCs are out of phase with each other, thus excluding possible contribution of the system artifact to the polarizer angle dependence. This linear polarization was observed in 34 of the 63 single $FAPbBr_3$ NCs studied in our experiment, while the other 29 showed no such behavior as can be seen in Fig. 2(c) for another single $FAPbBr_3$ NC. The degree of linear polarization (DLP) for a single $FAPbBr_3$ NC can be defined as $DLP = \frac{I_{max} - I_{min}}{I_{max} + I_{min}}$, where I_{max} and I_{min} are the maximum and minimum PL intensities, respectively. In Fig. 2(d), we plot a statistical histogram for the DLP distribution of the 34 single $FAPbBr_3$ NCs with polarized optical emission, where an average value of 11.24 ± 4.74% can be obtained. As discussed later in the text, the linearly-polarized optical emission of a single $FAPbBr_3$ NC should originate from the 1D dipole moment of a bright-exciton state. When this dipole moment is perpendicular (parallel) to the objective optical axis, a maximum (minimum) value of DLP would be expected [38–40]. When a single $FAPbBr_3$ NC is spin-coated onto the substrate, most likely its dipole moment could be lying between the above two extreme cases, which is one of the main factors to cause large variations in the measured DLP values.

According to previous studies in the literature [40–45], a reduction

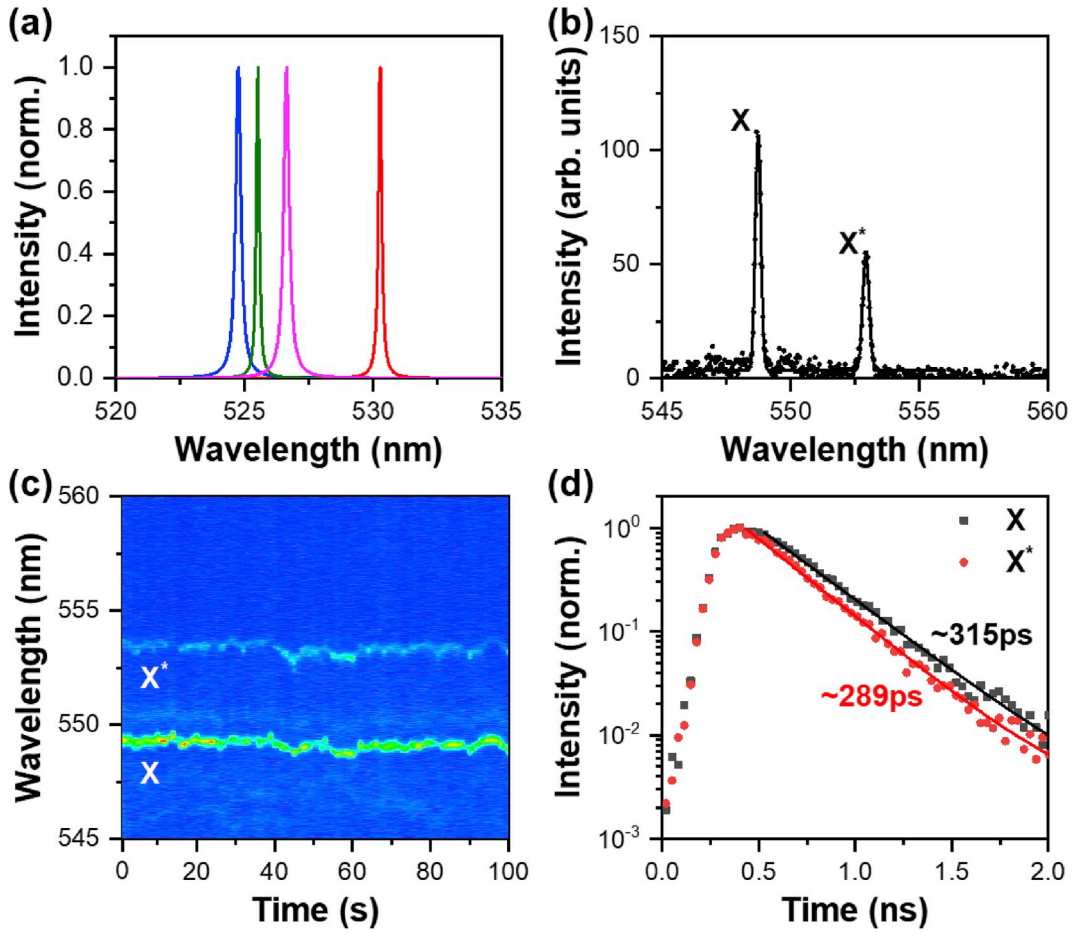

Fig. 3. (a) PL spectra of four single $FAPbBr_3$ NCs with different peak wavelengths. (b) PL spectrum measured for a single $FAPbBr_3$ NC with the PL peaks from both neutral (X) and charged (X*) single excitons. (c) Time-dependent PL spectral image measured for this single $FAPbBr_3$ NC where the X and X* PL peaks demonstrate synchronous spectral diffusion. (d) PL decay curves measured for the X and X* PL peaks of the same single $FAPbBr_3$ NC, and are fitted with single-exponential lifetimes of ~315 and ~289 ps, respectively. All the above optical measurements were performed at 4 K, and an integration time of 5 s was used for measuring each PL spectrum in (a)–(c).

of the crystal symmetry could yield asymmetric optical properties of semiconductor nanostructures. More specifically, the induced long-range electron-hole exchange interaction or Rashba effect is adequate to lift the exciton-state degeneracy, leading to fine-structure splittings that are intimately related to the linearly-polarized optical emission [20,44,46]. In the single $FAPbBr_3$ NCs studied here, the crystal structure would be distorted by the large organic cation of FA^+, causing transitions from the cubic to the tetragonal and orthorhombic phases at the room and cryogenic temperatures, respectively [31]. In lead-halide perovskites, the highest valence band is contributed by the *p* and *s* orbitals of X and Pb atoms, respectively, while the lowest conduction band by the *p* orbital of Pb atom [47]. Consequently, the band structure is mainly determined by the bond angle of Pb-X-Pb, the closer value of which to 180° would lead to smaller energy bandgap due to weaker orbital hybridization between the Pb and halide atoms. It was calculated previously for $MAPbI_3$ that, in both tetragonal and orthorhombic crystal structures, the bond angles of Pb–I–Pb in the apical direction is larger than that in the equatorial direction [48]. Therefore, the exciton-state energies for the 2D dipole moments in the equatorial direction (*x*-*y* plane) is higher than that for the 1D dipole moment in the apical direction (*z* axis), leading to a higher probability for exciton occupation of the lowest-energy state with linearly-polarized optical emission. Depending on the energy separation between the 2D and 1D bright-exciton states, their thermal mixing would vary from NC to NC, which should be another contributing factor to the partial linear polarization and the large distribution of DLP values observed in our experiment.

The energy-level splitting between the 1D and 2D exciton states can be roughly estimated from the DLP values measured in our experiment. At the room temperature, the 1D excitons could be populated to the upper 2D exciton state by thermal excitation. According to the Boltzmann distribution, the population ratio between the lower 1D (P_{lower}) and upper 2D (P_{upper}) exciton states is $\frac{P_{lower}}{P_{upper}} = e^{\frac{\Delta}{kT}}$, where Δ is the energy splitting, k is the Boltzmann's constant and T is the temperature. The DLP is connected with the exciton population by $\text{DLP} = \frac{P_{lower}-P_{upper}}{P_{lower}+P_{upper}} = \frac{e^{\frac{\Delta}{kT}}-1}{e^{\frac{\Delta}{kT}}+1}$. Since the measured DLP values might be underestimated when the dipole moment of 1D exciton is not perpendicular to the objective optical axis, we take the maximum value of ~21% instead of the average one of ~11% for the estimation of the energy-level splitting. By setting $\text{DLP} = \frac{e^{\frac{\Delta}{kT}}-1}{e^{\frac{\Delta}{kT}}+1} = 21\%$, we can obtain a maximum value of ~10 meV for the energy-level splitting Δ between the 1D and 2D exciton states. The $FAPbBr_3$ NCs studied in previous reports [31,32] normally have a cubic shape with a side length around 10 nm, and their exciton fine-structure splittings were observed to be several meV. In contrast, the $FAPbBr_3$ NCs used in our current experiment have a side length of ~12 nm, and some of them are apparently elongated (see the inset of Fig. 1(a)). It is likely that the large side length and the asymmetric shape are playing a joint role to determine the energy-level splitting between the 2D and 1D exciton states, which might deserve future theoretical considerations.

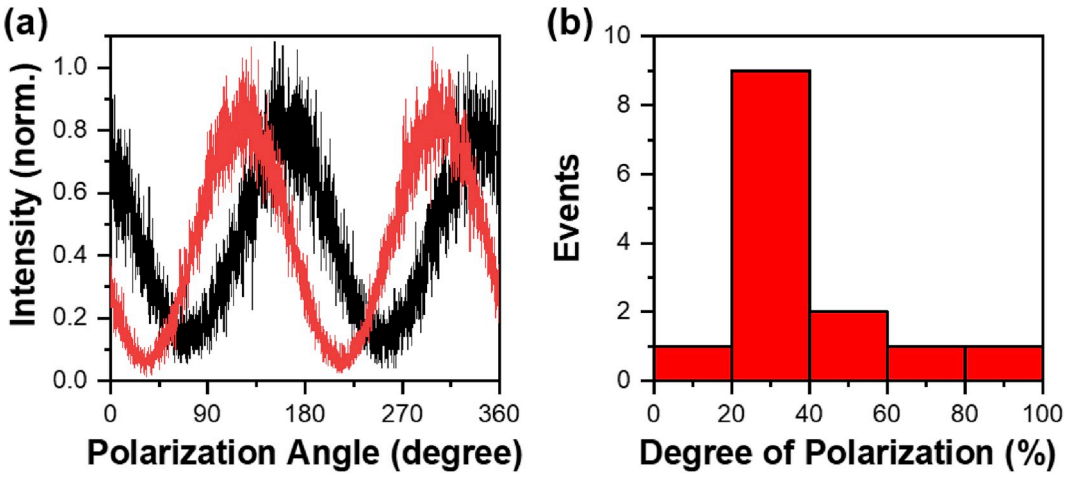

Fig. 4. (a) PL intensities measured at 4 K for two single $FAPbBr_3$ NCs showing obvious sinusoidal modulations with the changing polarizer angles. The DLP values are estimated to be ~78% (black curve) and ~92% (red curve), respectively, which are among the highest values for the single $FAPbBr_3$ NCs studied in our experiment. (b) Statistical histogram showing the degree of linear polarization values measured for 14 single $FAPbBr_3$ NCs at 4 K.

After the room-temperature measurements, we then switched to the cryogenic temperature of 4 K to gain a better understanding of the intrinsic optical properties of single $FAPbBr_3$ NCs. In Fig. 3(a), we plot the PL spectra measured for four single $FAPbBr_3$ NCs with different peak wavelengths, which should be dictated by the quantum confinement effect due to the size variations. With the low-power laser excitation at $<N> = 0.1$, most of the studied single $FAPbBr_3$ NCs possessed a single PL peak with an average linewidth of ~774 μeV, which should be caused by the fast spectral diffusion process discussed below. Occasionally, we could resolve an additional PL peak (denoted by X*) with a red-shifted energy relative to the main one (denoted by X), as can be seen in Fig. 3(b) from the PL spectrum of a representative single $FAPbBr_3$ NC. From the time-dependent PL spectral image shown in Fig. 3(c) for the same single $FAPbBr_3$ NC, the X* peak can be attributed to the charged-exciton emission since its spectral diffusion is synchronous to that of the main X peak from neutral excitons. The energy separation between the X and X* PL peaks in Fig. 3(b) and (c) is estimated to be ~17 meV, and this binding energy of charged excitons is consistent with those values obtained previously from single $CsPbBr_3$ NCs [17]. In Fig. 3(d), we plot the PL decay curves measured for the X and X* peaks of the same single $FAPbBr_3$ NC, which can both be fitted well by single-exponential functions to yield the exciton recombination lifetimes of ~315 and ~289 ps, respectively.

In the last experiment, we performed polarization-dependent measurements on single $FAPbBr_3$ NCs at 4 K, which all exhibited linearly-polarized feature in the optical emission. In Fig. 4(a), we plot the PL intensities of two single $FAPbBr_3$ NCs measured as a function of the polarizer angles, from which the respective DLP values of ~78% and ~92% can be estimated. For the 14 single $FAPbBr_3$ NCs studied, an average of 37.00 ± 20.91% can be obtained from their DLP values, which are presented in the statistical histogram of Fig. 4(b). Compared to the room-temperature value of 11.24%, this significantly enhanced DLP reflects the reduced thermal mixing between the exciton states carrying 2D and 1D dipole moments at the cryogenic temperature. In the previous study of single $CsPbBr_2Cl$ NCs with three bright-exciton states, the appearance of single- or double-line PL spectrum was explained in a scenario where the one or two upper exciton states were not thermally populated at 5 K [20]. In our case with single $FAPbBr_3$ NCs, the sizable DLP can be observed already at the room temperature, suggesting an even larger energy separation up to ~10 meV between the double 2D and single 1D exciton states.

4. Conclusion

To summarize, we have performed detailed optical characterizations of single perovskite $FAPbBr_3$ NCs, mainly focusing on single-photon emission, absorption cross section, exciton recombination lifetime, charged-exciton emission and PL spectral linewidth. While the above optical properties are on a par with those already possessed by other types of single perovskite NCs, linearly-polarized optical emission was demonstrated by single $FAPbBr_3$ NCs at both the room and cryogenic temperatures. We propose that this polarized emission originates from exciton recombination in a lower-lying state with 1D dipole moment, whose energy separation from the other two higher-lying states with 2D dipole moments could be as large as ~10 meV due to effective distortion of the Pb–I–Pb bond angle by the large organic cation of FA^+. The above findings have provided a deep understanding of the exciton energy-level structures of perovskite NCs, which could be influenced by the composing materials and the associated structure distortions. In practice, the polarized optical emission from perovskite NCs especially at room temperature can be utilized to favor various polarization-sensitive absorption and emission schemes, such as in photo-detectors, light-emitting diodes and lasers.

CRediT authorship contribution statement

Jinqiu Liu: Investigation, Writing - original draft, Visualization. **Fengrui Hu:** Investigation, Writing - original draft. **Yong Zhou:** Resources. **Chunfeng Zhang:** Resources. **Xiaoyong Wang:** Conceptualization, Writing - review & editing. **Min Xiao:** Conceptualization, Writing - review & editing.

Acknowledgements

This work is supported by the National Basic Research Program of China (2019YFA0308704 and 2017YFA0303700), the National Natural Science Foundation of China (61974058, 11574147 and 11621091), and the PAPD of Jiangsu Higher Education Institutions.

Appendix A. Supplementary data

Supplementary data to this article can be found online at https://doi.org/10.1016/j.jlumin.2020.117032.

References

[1] L.C. Schmidt, A. Pertegas, S. Gonzalez-Carrero, O. Malinkiewicz, S. Agouram, G. M. Espallargas, H.J. Bolink, R.E. Galian, J. Perez-Prieto, J. Am. Chem. Soc. 136 (2014) 850.
[2] L. Protesescu, S. Yakunin, M.I. Bodnarchuk, F. Bertolotti, N. Masciocchi, A. Guagliardi, M.V. Kovalenko, J. Am. Chem. Soc. 138 (2016) 14202.
[3] L. Protesescu, S. Yakunin, M.I. Bodnarchuk, F. Krieg, R. Caputo, C.H. Hendon, R. X. Yang, A. Walsh, M.V. Kovalenko, Nano Lett. 15 (2015) 3692.
[4] I. Levchuk, A. Osvet, X. Tang, M. Brandl, J.D. Perea, F. Hoegl, G.J. Matt, R. Hock, M. Batentschuk, C.J. Brabec, Nano Lett. 17 (2017) 2765.
[5] D.N. Minh, J. Kim, J. Hyon, J.H. Sim, H.H. Sowlih, C. Seo, J. Nam, S. Eom, S. Suk, S. Lee, E. Kim, Y. Kang, Chem. Mater. 29 (2017) 5713.
[6] F. Zhang, H.Z. Zhong, C. Chen, X.G. Wu, X.M. Hu, H.L. Huang, J.B. Han, B.S. Zou, Y.P. Dong, ACS Nano 9 (2015) 4533.
[7] Q.A. Akkerman, V. D'Innocenzo, S. Accornero, A. Scarpellini, A. Petrozza, M. Prato, L. Manna, J. Am. Chem. Soc. 137 (2015) 10276.
[8] G. Nedelcu, L. Protesescu, S. Yakunin, M.I. Bodnarchuk, M.J. Grotevent, M. V. Kovalenko, Nano Lett. 15 (2015) 5635.
[9] Y. Dong, T. Qiao, D. Kim, D. Parobek, D. Rossi, D.H. Son, Nano Lett. 18 (2018) 3716.
[10] W. Liu, Q. Lin, H. Li, K. Wu, I. Robel, J.M. Pietryga, V.I. Klimov, J. Am. Chem. Soc. 138 (2016) 14954.
[11] N.S. Makarov, S. Guo, O. Isaienko, W. Liu, I. Robel, V.I. Klimov, Nano Lett. 16 (2016) 2349.
[12] N. Yarita, H. Tahara, T. Ihara, T. Kawawaki, R. Sato, M. Saruyama, T. Teranishi, Y. Kanemitsu, J. Phys. Chem. Lett. 8 (2017) 1413.
[13] G. Raino, G. Nedelcu, L. Protesescu, M.I. Bodnarchuk, M.V. Kovalenko, R.F. Mahrt, T. Stoferle, ACS Nano 10 (2016) 2485.
[14] F. Hu, C. Yin, H. Zhang, C. Sun, W.W. Yu, C. Zhang, X. Wang, Y. Zhang, M. Xiao, Nano Lett. 16 (2016) 6425.
[15] Y.S. Park, S.J. Guo, N.S. Makarov, V.I. Klimov, ACS Nano 9 (2015) 10386.
[16] F. Hu, H. Zhang, C. Sun, C. Yin, B. Lv, C. Zhang, W.W. Yu, X. Wang, Y. Zhang, M. Xiao, ACS Nano 9 (2015) 12410.
[17] M. Fu, P. Tamarat, H. Huang, J. Even, A.L. Rogach, B. Lounis, Nano Lett. 17 (2017) 2895.
[18] M. Isarov, L.Z. Tan, M.I. Bodnarchuk, M.V. Kovalenko, A.M. Rappe, E. Lifshitz, Nano Lett. 17 (2017) 5020.
[19] C. Yin, L. Chen, N. Song, Y. Lv, F. Hu, C. Sun, W.W. Yu, C. Zhang, X. Wang, Y. Zhang, M. Xiao, Phys. Rev. Lett. 119 (2017), 026401.
[20] M.A. Becker, R. Vaxenburg, G. Nedelcu, P.C. Sercel, A. Shabaev, M.J. Mehl, J. G. Michopoulos, S.G. Lambrakos, N. Bernstein, J.L. Lyons, T. Stoferle, R.F. Mahrt, M.V. Kovalenko, D.J. Norris, G. Raino, A.L. Efros, Nature 553 (2018) 189.
[21] P.C. Sercel, J.L. Lyons, D. Wickramaratne, R. Vaxenburg, N. Bernstein, A.L. Efros, Nano Lett. 19 (2019) 4068.
[22] R. Ben Aich, I. Saïdi, S. Ben Radhia, K. Boujdaria, T. Barisien, L. Legrand, F. Bernardot, M. Chamarro, C. Testelin, Phys. Rev. Appl. 11 (2019), 034042.
[23] S. Yakunin, L. Protesescu, F. Krieg, M.I. Bodnarchuk, G. Nedelcu, M. Humer, G. De Luca, M. Fiebig, W. Heiss, M.V. Kovalenko, Nat. Commun. 6 (2015) 8056.
[24] Y. Wang, X. Li, J. Song, L. Xiao, H. Zeng, H. Sun, Adv. Mater. 27 (2015) 7101.
[25] Y. Xu, Q. Chen, C. Zhang, R. Wang, H. Wu, X. Zhang, G. Xing, W.W. Yu, X. Wang, Y. Zhang, M. Xiao, J. Am. Chem. Soc. 138 (2016) 3761.
[26] X. Zhang, H. Lin, H. Huang, C. Reckmeier, Y. Zhang, W.C. Choy, A.L. Rogach, Nano Lett. 16 (2016) 1415.
[27] J. Song, J. Li, X. Li, L. Xu, Y. Dong, H. Zeng, Adv. Mater. 27 (2015) 7162.
[28] L. Protesescu, S. Yakunin, S. Kumar, J. Bar, F. Bertolotti, N. Masciocchi, A. Guagliardi, M. Grotevent, I. Shorubalko, M.I. Bodnarchuk, C.J. Shih, M. V. Kovalenko, ACS Nano 11 (2017) 3119.
[29] N. Yarita, H. Tahara, M. Saruyama, T. Kawawaki, R. Sato, T. Teranishi, Y. Kanemitsu, J. Phys. Chem. Lett. 8 (2017) 6041.
[30] C.T. Trinh, D.N. Minh, K.J. Ahn, Y. Kang, K.-G. Lee, ACS Photonics 5 (2018) 4937.
[31] O. Pfingsten, J. Klein, L. Protesescu, M.I. Bodnarchuk, M.V. Kovalenko, G. Bacher, Nano Lett. 18 (2018) 4440.
[32] P. Tamarat, M.I. Bodnarchuk, J.B. Trebbia, R. Erni, M.V. Kovalenko, J. Even, B. Lounis, Nat. Mater. 18 (2019) 717.
[33] N. Yarita, T. Aharen, H. Tahara, M. Saruyama, T. Kawawaki, R. Sato, T. Teranishi, Y. Kanemitsu, Phys. Rev. Mater. 2 (2018) 116003.
[34] M. Fu, P. Tamarat, J.B. Trebbia, M.I. Bodnarchuk, M.V. Kovalenko, J. Even, B. Lounis, Nat. Commun. 9 (2018) 3318.
[35] L. Chen, B. Li, C. Zhang, X. Huang, X. Wang, M. Xiao, Nano Lett. 18 (2018) 2074.
[36] P. Senellart, G. Solomon, A. White, Nat. Nanotechnol. 12 (2017) 1026.
[37] H. Utzat, W.W. Sun, A.E.K. Kaplan, F. Krieg, M. Ginterseder, B. Spokoyny, N. D. Klein, K.E. Shulenberger, C.F. Perkinson, M.V. Kovalenko, M.G. Bawendi, Science 363 (2019) 1068.
[38] S.A. Empedocles, R. Neuhauser, M.G. Bawendi, Nature 399 (1999) 126.
[39] C. Lethiec, J. Laverdant, H. Vallon, C. Javaux, B. Dubertret, J.-M. Frigerio, C. Schwob, L. Coolen, A. Maître, Phys. Rev. X 4 (2014), 021037.
[40] S. Vezzoli, M. Monceau, G. Lemenager, Q. Glorieux, E. Giacobino, L. Carbone, M. De Vittorio, A. Bramati, ACS Nano 9 (2015) 7992.
[41] D. Wang, D. Wu, D. Dong, W. Chen, J. Hao, J. Qin, B. Xu, K. Wang, X. Sun, Nanoscale 8 (2016) 11565.
[42] A.L. Efros, Phys. Rev. B 46 (1992) 7448.
[43] T. Ihara, R. Sato, T. Teranishi, Y. Kanemitsu, Phys. Rev. B 90 (2014), 035309.
[44] D. Tauber, A. Dobrovolsky, R. Camacho, I.G. Scheblykin, Nano Lett. 16 (2016) 5087.
[45] Z.-F. Shi, Y. Li, S. Li, H.-F. Ji, L.-Z. Lei, D. Wu, T.-T. Xu, J.-M. Xu, Y.-T. Tian, X.-J. Li, J. Mater. Chem. C 5 (2017) 8699.
[46] M. Bayer, G. Ortner, O. Stern, A. Kuther, A.A. Gorbunov, A. Forchel, P. Hawrylak, S. Fafard, K. Hinzer, T.L. Reinecke, S.N. Walck, J.P. Reithmaier, F. Klopf, F. Schäfer, Phys. Rev. B 65 (2002) 195315.
[47] M.R. Filip, G.E. Eperon, H.J. Snaith, F. Giustino, Nat. Commun. 5 (2014) 5757.
[48] W. Geng, L. Zhang, Y.-N. Zhang, W.-M. Lau, L.-M. Liu, J. Phys. Chem. C 118 (2014) 19565.